J. Phys. B: At. Mol. Opt. Phys. **32** (1999) 5123–5146. Printed in the UK PII: S0953-4075(99)04974-3

Differential cross sections for electron-impact excitation out of the metastable levels of the barium atom

P W Zetner†, S Trajmar‡, I Kanik‡, S Wang‡, G Csanak§, R E H Clark§, J Abdallah Jr§, D Fursa‖ and I Bray‖

† Department of Physics and Astronomy, University of Manitoba, Winnipeg, MB, Canada R3T 2N2

‡ Jet Propulsion Laboratory, 4800 Oak Grove Drive, MS 183-601 Pasadena, CA 91109, USA

§ Los Alamos National Laboratory, Theoretical Division, MS B-212 Los Alamos, NM 87545, USA

‖ School of Physical Sciences, Flinders University of South Australia GPO Box 2100, Adelaide 5001, Australia

Received 8 June 1999

Abstract. We report an experimental and theoretical investigation of low-energy electron scattering from ^{138}Ba atoms prepared in the metastable $^3D_2$ and $^1D_2$ levels by laser-optical pumping. Differential cross sections were measured for excitation out of these metastable levels to a variety of higher-lying levels at electron-impact energies of 10, 20 and 36.7 eV. A comparison of experimental data with the results of theoretical approaches using the unitarized distorted-wave approximation and the convergent close-coupling scheme is given.

1. Introduction

Electron collisions with excited atoms have been characterized far less extensively than collisions with ground-state atoms because of the relative difficulty of experimental and theoretical methods applied to their study. From a practical standpoint, the investigation of such collision processes is important because of the ubiquitous presence of excited species in partially ionized plasmas (e.g. high-density gas discharges (Krivchenkova and Khakaev 1975, Delcroix *et al* 1976, Massey *et al* 1982a), astrophysical plasmas (Allen 1984), auroral plasmas (Massey *et al* 1982b) and electron-beam and discharge-pumped lasers (Massey *et al* 1982c)). Collision processes involving excited metastable species are particularly important because significant populations of these can accumulate in such plasma systems. Review papers by Trajmar and Nickel (1992) and Lin and Anderson (1992) have summarized the available data and have emphasized the rather deficient state of our knowledge of scattering processes involving excited atoms. Growing experimental and theoretical interest in the problem has, however, resulted in some additional work since the publication of these reviews. Electron-impact ionization of rare-gas metastable atoms has been studied by Johnston *et al* (1996). Integral cross sections (ICS) for electron-impact excitation out of the metastable levels of calcium have been reported (Shafranyosh *et al* 1997). Differential cross sections (DCS) and electron-impact coherence parameters (EICP) for the excitation of the barium (...6s6p $^1P_1$) state out of the $^1D_2$ metastable level have also been reported (Li and Zetner 1995, 1996, Johnson *et al* 1999). Inner-shell ionization of metastable barium atoms has been studied by Azizi *et al* (1994).

0953-4075/99/215123+24$30.00

This paper is concerned with electron collisions on the metastable ^{1}D and ^{3}D levels of the barium atom. We have determined differential cross sections for excitations of the type $^1\mathrm{D} \rightarrow \mathrm{X}$, $^3\mathrm{D} \rightarrow \mathrm{X}$ where X represents some higher-lying atomic level. From an experimental standpoint, barium represents an ideal target with which to investigate scattering from excited atoms. When CW laser radiation tuned to the $^1\mathrm{S}_0$–$^1\mathrm{P}_1$ resonance transition wavelength of 553.7 nm interacts with a beam of barium vapour, significant populations of atoms in the (. . . 6s6p $^1\mathrm{P}_1$) level can be produced. This P level is short-lived (with a lifetime of 8.37 ns as reported by Kelley and Mathur (1977)) and decays to the ground state as well as the (. . . 6s5d ^{1}D, ^{3}D) metastable levels. Although branching into the metastable levels is weak (as described in more detail below), large populations of these species can develop through optical pumping under typical experimental conditions. Achievable metastable atom concentrations of the order of 10^{10}–10^{11} cm^{-3} are sufficient to carry out reliable DCS measurements, at least for the stronger excitations.

In a previous paper (Zetner *et al* 1997), we demonstrated the feasibility of this approach by presenting measured DCS for electron-impact excitation of a large number of atomic levels out of the laser-excited (. . . 6s6p $^1\mathrm{P}_1$) level. This work also demonstrated that theoretical approaches to the problem of electron scattering from excited atoms have advanced to the point where meaningful comparison with measured data can be made. In particular, the unitarized distorted-wave approximation (UDWA) was shown to be reasonably effective in describing the stronger, dipole-allowed excitations out of the (. . . 6s6p $^1\mathrm{P}_1$) state. This paper will compare measured DCS for excitation out of the metastable ^{1}D, ^{3}D levels with theory based on the UDWA formalism as well as the convergent close-coupling (CCC) scheme. The CCC approach has recently been shown (Fursa and Bray 1999) to give excellent agreement with measured DCS and EICP for the $^1\mathrm{S}_0$ to $^1\mathrm{P}_1$ excitation. Perhaps of more interest in the context of electron scattering from excited Ba atoms is the paper by Johnson *et al* (1999) in which the comparison of measurement and CCC theory for the (. . . 6s5d $^1\mathrm{D}_2$)–(. . . 6s6p $^1\mathrm{P}_1$) excitation reveals good agreement and the work of Trajmar *et al* (1998, 1999) in which the CCC theory is applied to elastic scattering from the excited D and P levels. Our goal in the present investigation is to evaluate the UDWA and CCC schemes in their ability to describe a variety of excitations $^1\mathrm{D}, {}^3\mathrm{D} \rightarrow \mathrm{X}$ where X represents a higher-lying atomic level.

2. Measurement of the differential cross sections

The crossed-beam apparatus used to carry out the measurements has been described in detail by Zetner *et al* (1997). It consists of an electron energy-loss spectrometer operated at approximately 50 meV system energy resolution with an angular resolution of about 2°. Typical electron-beam currents of about 10 nA were attained. A resistively heated oven provided a collimated (beam divergence of about ±6°) barium vapour beam with an estimated target density of 10^{11} cm^{-3} at the interaction region. The apparatus was designed to give a horizontal scattering plane (as defined by the electron gun and detector axes) with the oven emitting barium vapour vertically upwards. The isotopic composition of the barium sample is given by the natural isotopic abundances where isotopes of atomic weight (138, 137, 136, 135, 134) are present in the fractional amounts (0.717, 0.113, 0.078, 0.066, 0.024), respectively.

Laser radiation of 50–80 mW in intensity, tuned to the $^1\mathrm{S}_0$–$^1\mathrm{P}_1$ resonance transition in ^{138}Ba at 553.7 nm, was injected into the apparatus in a horizontal direction, intersecting the barium vapour beam perpendicularly at a point between the oven and the scattering-interaction region (roughly 5 mm below the scattering plane). We will refer to the volume of intersection of the barium vapour beam and the laser beam as the laser-pumping region. In our previous work

(Zetner *et al* 1997), we designated this arrangement of distinct laser-pumping and scattering-interaction regions as the 'laser-low' geometry.

The laser beam was set to an incidence direction of 45° with respect to the electron-beam direction and a linear polarization at 54.7° with respect to the horizontal. Tuning to the S–P transition in the ^{138}Ba was easily accomplished by visual observation of resonance fluorescence from the vapour beam. The appropriate conditions on atom beam collimation, laser-beam divergence, laser-beam intensity, etc required to selectively excite the $^1S_0$–$^1P_1$ transition in ^{138}Ba have been discussed in detail by Register *et al* (1983). In the absence of radiation-trapping effects, we estimate a combined homogeneously and inhomogeneously broadened absorption linewidth of approximately 140 MHz in our case; sufficient to isolate the ^{138}Ba isotope for optical pumping. We note that, for our present purposes, it is not crucial to selectively isolate the ^{138}Ba isotope for optical excitation as discussed below.

Through the process of radiative cascade from the $^1P_1$ level, substantial populations of ^{138}Ba (...6s5d $^1D_2$) and (...6s5d $^3D_2$) metastable atoms are produced along with a relatively small concentration of atoms in the (...6s5d $^3D_1$) level. These metastable atoms are long-lived and drift out of the laser-pumping region into the scattering-interaction region. As a result, the target beam at the interaction region comprises a mixture of ground- and excited-state species: ground-state atoms of both even and odd isotopes along with ^{138}Ba (...6s5d $^1D_2$, $^3D_2$, $^3D_1$) atoms. The ^{138}Ba (...6s6p $^1P_1$) atoms quickly decay as they exit the laser-pumping region and are consequently not present as a target beam constituent in the interaction region. We assume the population ratios of the excited metastable species to be determined by the branching fractions for radiative cascade from the $^1P_1$ level. These have been measured by Bizzari and Huber (1990) to be 9.97×10^{-1}, 9.0×10^{-4}, 2.6×10^{-5} and 2.06×10^{-3} for optical transitions terminating on the $^1S_0$, $^3D_2$, $^3D_1$ and $^1D_2$ levels, respectively. Based on the small value measured for branching into the $^3D_1$ level, we ignore atoms excited to this level as a target constituent.

The well defined polarization state and incidence direction of the laser beam give rise to a $^1P_1$ state which is, in general, aligned or oriented. Following Blum (1981), an atomic population is defined to be aligned or oriented if the population distribution over magnetic sublevels is anisotropic. If μ denotes the magnetic quantum number of a magnetic sublevel $|\mu\rangle$ then the anisotropic population is said to be aligned when the populations in sublevels $|\mu\rangle$ and $|-\mu\rangle$ are the same or oriented if the populations in $|\mu\rangle$ and $|-\mu\rangle$ are different. Radiative cascade from the aligned/oriented $^1P_1$ state can transfer some of this alignment/orientation to the lower level because the optical selection rules are magnetic sublevel dependent. Since electron-scattering processes are generally dependent on alignment/orientation, it therefore becomes necessary to quantify the magnetic sublevel anisotropy in the atomic target population.

The scattering intensity, I, from an aligned/oriented target can be written (Macek and Hertel 1974) as

$$I = C\,\mathrm{Tr}[\hat{\rho}\hat{\tau}] \tag{1}$$

where $\mathrm{Tr}[\hat{\rho}\hat{\tau}]$ represents the trace of the product of two density operators, $\hat{\rho}$ and $\hat{\tau}$. The density operator $\hat{\tau}$ describes the aligned/oriented initial atomic target population which, in the present studies, corresponds to the cascade-populated ($J = 2$) ^{1}D or ^{3}D atom. The density operator $\hat{\rho}$ is determined by scattering amplitudes $\langle m|\hat{T}|\mu\rangle$ which couple magnetic substates, $|\mu\rangle$, in the D level to magnetic substates $|m\rangle$ in some final level (X) through the action of a transition operator, $\hat{T}$, representing the electron-impact excitation. The constant C contains factors such as target number density, incident electron-beam current, effective scattering volume, etc. The density operator $\hat{\rho}$ can be expressed in terms of spherical tensor multipoles $T_{kq}^{(\mathrm{col})}$ for the collisionally excited atomic population, while the density operator $\tilde{\tau}$ can be written in terms of spherical

tensor multipoles $T_{kq}^{(a)}(D)$ for the cascade-populated $J = 2$, D level atomic population (see Blum 1981, for example). For linearly polarized laser light propagating in the scattering plane, it can be shown that

$$I = \overline{C}\left\{ T_{00}^{(a)}(D)T_{00}^{(col)} + T_{20}^{(a)}(D)\begin{bmatrix} T_{22}^{(col)}\sqrt{\frac{3}{2}}(\cos^2\theta_v\cos^2\psi - \sin^2\psi) \\ \pm T_{21}^{(col)}\sqrt{\frac{3}{2}}\sin(2\theta_v)\cos^2\psi \\ +T_{20}^{(col)}\frac{1}{2}(3\sin^2\theta_v\cos^2\psi - 1) \end{bmatrix}\right\} \tag{2}$$

where θ_v gives the angle of the laser-beam propagation direction with respect to the incident electron beam and ψ gives the direction of linear polarization with respect to the scattering plane. The sign of the term involving $T_{21}^{(col)}$ is positive (negative) for electron scattering to the left (right), respectively. For our case of linearly polarized light, only alignment (no orientation) is produced in the target. Note that, for an isotropic (i.e. unaligned/unoriented) target, only $T_{00}^{(a)}(D)$ is non-zero and the scattering intensity, I, becomes proportional to the DCS.

Under our experimental conditions, we have observed a small dependence of electron-scattering intensity on laser polarization (for a number of representative excitations $^1D_2$–X) when the laser-pumping region and the scattering-interaction region overlap (the 'laser-centre' geometry of Zetner *et al* (1997)). This dependence was much smaller than that observed for excitations out of the $^1P_1$ state (Zetner *et al* 1997) which can be understood upon comparison of the atomic target state multipoles for the laser-excited P state, $T_{kq}^{(a)}(P)$, and the cascade-populated D level, $T_{kq}^{(a)}(D)$. These are given by (Korenman 1975)

$$T_{kq}^{(a)}(D) = T_{kq}^{(a)}(P)\beta_k(P \rightarrow D, 1) \tag{3}$$

where

$$\beta_k(L_a \rightarrow L_b, L) = (2L+1)(-1)^{L_a+L_b+L+k}\begin{Bmatrix} L & L_a & L_b \\ k & L_b & L_a \end{Bmatrix}.$$

In the laser-photon frame (with the quantization axis along the linear polarization direction), it can be shown that $\beta_2 = \sqrt{21}/10$. The observed scattering intensity, for excitations out of the D levels, will, therefore, show less polarization dependence than for excitations out of the P level by at least a factor of two. For the laser-low geometry utilized in the present scattering studies, we observed that the polarization dependence of the electron-scattering signal was negligibly small.

We attribute the loss of polarization dependence in the laser-low arrangement to radiation-trapping effects which convert an initially anisotropic D level population to an isotropic population as the metastables drift to the interaction region. This conversion presumably occurs by the following means. Although the laser-pumping region is well defined by the laser beam–atom beam overlap, scattered-resonance radiation is visible along the barium-vapour beam outside of this pumping region. The intensity of this scattered radiation is weak but the atom–photon interaction length, extending from the oven orifice to the scattering-interaction region (approximately 5 mm distance) is large. The successive absorptions and re-emissions of resonant radiation, which are responsible for this scattered light, will also tend to randomize the directions and polarizations of resonant photons interacting with barium atoms as they drift to the scattering region. Consequently, we expect a significant reduction in the alignment of the target population of metastable D level atoms arriving at the scattering region.

Furthermore, randomization of the photon directions in the atomic-vapour beam will spoil the selectivity required to isolate the ^{138}Ba isotope for optical excitation, as S–P transitions in the odd isotopes can become Doppler-shifted into resonance with the scattered photons. This

effect was measured by Azizi *et al* (1994) in a laser-beam 'pump and probe' technique applied to a barium vapour beam very similar to that employed here. In contrast to the even barium isotopes (for which the nuclear spin is $I = 0$), the odd isotope nuclear spins are non-zero ($I = \frac{5}{2}, \frac{3}{2}$ for ^{137}Ba, ^{135}Ba, respectively) leading to a level scheme complicated by hyperfine structure. Resonance transitions of the type $J = \frac{3}{2}, \frac{5}{2}$ to $J' = \frac{1}{2}, \frac{3}{5}, \frac{5}{2}$ in these isotopes would give rise to cascade-populated D level atoms which are essentially isotropic. According to the natural isotopic abundances, approximately 18% of the target metastable population could then be populated isotropically in this way. In this paper, we have treated the metastable D level atomic target population as isotropic and assumed that the scattering signal arising from a given excitation is proportional to the DCS for that excitation. This reasoning is consistent with the observations of Trajmar *et al* (1999) who found no laser-polarization dependence of the elastic-scattering signal from metastable (^{1}D, ^{3}D) barium atoms in a similar experimental arrangement.

Our measurement procedure involved the following sequence of steps. For a particular impact energy, E_0, and scattering angle, θ, of interest, energy loss spectra were produced in the laser-low geometry and in laser-off mode under identical experimental conditions. This was accomplished with a laser-beam blocking shutter under computer control. Features in the laser-low spectra are associated with excitations out of the ^{1}D and ^{3}D metastables to higher-lying levels, X, as well as ground-state excitations. The laser-off spectrum provided us with a means to subtract spectral features belonging to excitations out of the ground state from a 'laser-low' spectrum. Such a processed laser-low spectrum then contains excitations out of the metastable states only. In some cases, isolated features corresponding to specific excitations ^{1}D$_2$–X or ^{3}D$_2$–X could be identified and extracted with a spectrum-fitting routine. In other instances, well defined blended features could be identified. Table 1 gives a listing of the excitations associated with the strongest features present in our measured spectra. For a given scattering angle, θ, measurements were taken for both left- and right-hand scattering and the results were combined. To convert spectral feature intensities into cross sections, we made use of the (6s^2 ^{1}S$_0$)–(6s6p ^{1}P$_1$) inelastic feature intensity in the laser-off spectra. This allowed us to determine the relative metastable population in the target beam and provided a normalization factor to the known DCS for this transition (Jensen *et al* 1978, Wang *et al* 1994).

The normalization procedure consists of applying the equations

$$I(^1\mathrm{D}_2\text{–X}) = V^*_{\mathrm{eff}} N(^1\mathrm{D}_2)\mathrm{DCS}(^1\mathrm{D}_2\text{–X}) \tag{4a}$$

$$I(^3\mathrm{D}_2\text{–X}) = V^*_{\mathrm{eff}} N(^3\mathrm{D}_2)\mathrm{DCS}(^3\mathrm{D}_2\text{–X}) \tag{4b}$$

$$I(^1\mathrm{S}_0\text{–}^1\mathrm{P}_1) = V_{\mathrm{eff}} N(^1\mathrm{S}_0)\mathrm{DCS}(^1\mathrm{S}_0\text{–}^1\mathrm{P}_1) \tag{4c}$$

for the laser-low geometry, and

$$\left[I(^1\mathrm{S}_0\text{–}^1\mathrm{P}_1)\right]_{\mathrm{off}} = V_{\mathrm{eff}}\left[N(^1\mathrm{S}_0)\right]_{\mathrm{off}}\mathrm{DCS}(^1\mathrm{S}_0\text{–}^1\mathrm{P}_1) \tag{4d}$$

for the laser-off spectrum. Here, $I(\,)$ refers to the intensity of a spectral feature associated with the transition indicated in parentheses and DCS( ) is the associated differential cross section. The quantity $N(\,)$ refers to the population of target species indicated in the parentheses and V_{eff} and V^*_{eff} represent effective scattering volumes for ground- and excited-state atomic targets, respectively. The concept of the effective scattering volume has been discussed in detail by Brinkmann and Trajmar (1981). A constraint on the populations, $N(\,)$, is given by

$$\left[N(^1\mathrm{S}_0)\right]_{\mathrm{off}} = N(\mathrm{D}) + N(^1\mathrm{S}_0) \tag{5}$$

where $N(\mathrm{D}) = N(^1\mathrm{D}_2) + N(^3\mathrm{D}_2)$ is the population of atoms excited into any D level (ignoring the very small population of ^{3}D$_1$ produced).

Table 1.

Observed feature	Feature notation[a]	Associated level excitations[b]					
		Initial level[b]	Initial level number[a]	Final level[b]	Final level number[a]	Final level energy (eV)	Threshold excitation energy (eV)
a	21	$6s5d\ ^3D_2$	3	$6s6p\ ^3P_2$	7	1.675	0.533
b	22	$6s5d\ ^1D_2$	8	$6s6p\ ^1P_1$	9	2.239	0.826
c	23	$6s5d\ ^3D_2$	3	$6s6p\ ^1P_1$	9	2.239	1.097
d	24	$6s5d\ ^1D_2$	8	$6p5d\ ^3F_2$	13	2.736	1.323
e	25	$6s5d\ ^1D_2$	8	$6p5d\ ^3F_3$	16	2.845	1.432
	26a	$6s5d\ ^1D_2$	8	$5d^2\ ^1D_2$	17	2.859	1.446
	26b	$6s5d\ ^1D_2$	8	$6p5d\ ^1D_2$	14	2.861	1.448
	27	$6s5d\ ^1D_2$	8	$5d^2\ ^3P_1$	18	2.911	1.498
f	28	$6s5d\ ^1D_2$	8	$5d^2\ ^3P_2$	20	2.966	1.553
	29	$6s5d\ ^3D_2$	3	$6p5d\ ^3F_2$	13	2.736	1.594
	30	$6s5d\ ^1D_2$	8	$6p5d\ ^3D_2$	22	3.041	1.628
g	31	$6s5d\ ^3D_2$	3	$6p5d\ ^3F_3$	16	2.845	1.703
	32a	$6s5d\ ^3D_2$	3	$5d^2\ ^1D_2$	17	2.859	1.717
	32b	$6s5d\ ^3D_2$	3	$6p5d\ ^1D_2$	14	2.861	1.719
i_1	40	$6s5d\ ^3D_2$	3	$6p5d\ ^3P_1$	25	3.187	2.045
	41	$6s5d\ ^3D_2$	3	$6p5d\ ^3P_2$	27	3.218	2.076
i_2	42	$6s5d\ ^1D_2$	8	$6s7p\ ^1P_1{}^\dagger$	32	3.540	2.127

[a] Notation of Zetner *et al* (1997).

[b] Level designations indicate the dominant two-electron configuration as calculated in the HF scheme of Cowan (1968a, b, 1981) and Cowan and Griffin (1967). There is agreement with the designations of Moore (1958) in all cases except that identified by the superscript dagger. Final level energies and threshold excitation energies are based on the values of Moore (1958).

Using equations (5), (4*b*) and (4*c*) we obtain

$$\frac{N(\mathrm{D})}{N(^1\mathrm{S}_0)} = \frac{\left[I(^1\mathrm{S}_0{-}^1\mathrm{P}_1)\right]_{\mathrm{off}}}{I(^1\mathrm{S}_0{-}^1\mathrm{P}_1)} - 1 \tag{6}$$

for the relative population of excited metastable targets and we distribute this excited population into the two D levels using the branching fractions quoted earlier, to obtain

$$\frac{N(^1\mathrm{D}_2)}{N(^1\mathrm{S}_0)} = 0.70\frac{N(\mathrm{D})}{N(^1\mathrm{S}_0)} \tag{7a}$$

and

$$\frac{N(^3\mathrm{D}_2)}{N(^1\mathrm{S}_0)} = 0.30\frac{N(\mathrm{D})}{N(^1\mathrm{S}_0)}. \tag{7b}$$

To determine the cross section for a given excitation, we use

$$\mathrm{DCS}(^{1,3}\mathrm{D}_2{-}\mathrm{X}) = \frac{V_{\mathrm{eff}}}{V^*_{\mathrm{eff}}}\frac{N(^1\mathrm{S}_0)}{N(^{1,3}\mathrm{D}_2)}\frac{I(^{1,3}\mathrm{D}_2{-}\mathrm{X})}{I(^1\mathrm{S}_0{-}^1\mathrm{P}_1)}\mathrm{DCS}(^1\mathrm{S}_0{-}^1\mathrm{P}_1). \tag{8}$$

By ensuring that the laser-beam illumination is uniform over the entire atomic vapour beam in the laser-pumping region, we can enforce the condition $V_{\mathrm{eff}} = V^*_{\mathrm{eff}}$ to further simplify equation (8). Additional criteria for the validity of equation (8) are the assumption of a flat-detection response function for the range of scattered-electron residual energies associated with

the range of interest in the energy loss spectrum and the neglect of weak energy loss features arising from excitations out of the metastable levels which underlie the $^1S_0$–$^1P_1$ feature in the laser-low spectrum.

3. Theoretical methods

Differential cross sections were calculated using the unitarized distorted-wave approximation and the convergent close-coupling method. These are now discussed separately.

3.1. The UDWA approach

The UDWA method has been described by Mann (1983) and has been applied to the description of excitation out of the Ba(...6s6p $^1P_1$) level in Zetner *et al* (1997). In this approximation, the wavefunction of the incident continuum electron is calculated using the potential of the initial target state, while that of the scattered electron is calculated using the potential of the final target state. For the continuum electron, 350 and 390 partial waves were used for weak (optically forbidden) and strong (optically allowed) transitions, respectively. Unitarization of the matrix elements is performed (Saraph *et al* 1969, Davis *et al* 1976, Mann 1983 equation (4)). Transformation from LS to intermediate coupling and the inclusion of mixing of the target states is carried out in the pair-coupling scheme (Saraph 1972, Clark 1978, Mann 1983).

The collision calculation uses the energy levels, wavefunctions and mixing coefficients from a structure calculation based on the Hartree–Fock (HF) method as developed by Cowan (1968a, b, 1981) and Cowan and Griffin (1967). The radial wavefunctions are calculated one configuration at a time. The calculation is essentially non-relativistic except that the mass and Darwin terms are included. The radial wavefunctions minimize the configuration-average energy, not the LS-term energy. From mixing among all LS terms with the same parity and total angular momentum, J, we obtained (through diagonalization of the atomic Hamiltonian with the given basis set) the mixing coefficients, energy levels and radial wavefunctions which are then available for the collision calculations. A very thorough description of the HF method is given by Cowan (1981), so we will not repeat the details here.

In all scattering calculations, wavefunctions resulting from 22 configurations were used. The relevant configurations involved a Xe core ($1s^22s^22p^63s^23p^63d^{10}4s^24p^64d^{10}5s^25p^6$) with the addition of two valence electrons comprising the two-electron configurations: $6s^2$, $6p^2$, $5d^2$, 5d6d, 6p7p, 6s7s, 6s8s, 6s7d, 6s8d, 6s9d, 6s5d, 6s6d, 6s6p, 6p7s, 6p8s, 6p5d, 6p6d, 6p7d, 6p8d, 6s7p, 6s8p, 6s9p. The 139 levels obtained from these 22 configurations and the mixing coefficients for all 139 wavefunctions are available from the Los Alamos National Laboratory. Table 2 gives the configuration composition for the levels of interest here.

3.2. The CCC approach

The application of this method to the (...6s5d $^1D_2$)–(...6s6p $^1P_1$) excitation in barium has been described in Johnson *et al* (1999). We refer to Fursa and Bray (1997) for the details of the calculation of electron scattering from alkaline-earth atoms. Here, we give a brief overview of the method and details specific to e^-–Ba scattering. The CCC method is formulated in a non-relativistic LS coupling framework. The total wavefunction (projectile and target electrons) is expanded in a basis of barium target states. The close-coupling equations for the T-matrix (coupled Lippman–Schwinger equations) are then formulated and solved in momentum space.

For barium target states, we adopt a model of two valence electrons above an inert Hartree–Fock core. Standard configuration-interaction (CI) expansion has been used to obtain

Table 2. Configuration mixing coefficients used in the UDWA calculations.

Level:	3	7	8	9	13	14	17	18	18	20	22	25	27	32
J:	2	2	2	1	2	2	3	2	1	2	2	1	2	1
6s5d ^{3}D	0.9878	—	0.1554	—	—	—	—	—	—	—	—	—	—	—
^{1}D	−0.1479	—	0.9300	—	—	—	—	0.1131	—	0.0854	—	—	—	—
6s6p ^{3}P	—	0.9876	—	−0.0555	—	—	—	—	—	—	—	−0.1425	−0.1452	—
^{1}P	—	—	—	0.8424	—	—	—	—	—	—	—	−0.0561	—	0.2841
5d^2 ^{1}S	—	—	—	—	—	—	—	—	—	—	—	—	—	—
^{3}P	—	—	—	—	—	—	—	−0.5650	0.9175	0.7280	—	—	—	—
^{1}D	—	—	−0.2478	—	—	—	—	0.7012	—	0.5499	—	—	—	—
^{3}F	—	—	—	—	—	—	—	−0.1252	—	−0.0729	—	—	—	—
5d6p ^{3}P	—	0.1398	—	—	−0.0563	−0.0759	—	—	—	—	—	0.9729	0.9710	0.0874
^{1}P	—	—	—	−0.5253	—	—	—	—	—	—	—	−0.0563	—	0.5854
^{3}D	—	—	—	—	−0.0895	−0.1455	—	—	—	—	0.9844	—	—	—
^{1}D	—	—	—	—	0.6580	0.7275	—	—	—	—	0.1656	—	0.1003	—
^{3}F	—	—	—	—	0.7444	−0.6650	0.9980	—	—	—	—	—	—	—
^{1}F	—	—	—	—	—	—	—	—	—	—	—	—	—	—
6s7p ^{3}P	—	—	—	—	—	—	—	—	—	—	—	0.1324	0.1383	—
^{1}P	—	—	—	−0.0710	—	—	—	—	—	—	—	—	—	−0.7147
6s6d ^{1}D	—	—	—	—	—	—	—	−0.0878	—	−0.0740	—	—	—	—
6p^2 ^{1}S	—	—	—	—	—	—	—	—	—	—	—	—	—	—
^{3}P	—	—	—	—	—	—	—	−0.2358	0.3910	0.2991	—	—	—	—
^{1}D	—	—	0.2154	—	—	—	—	0.3009	—	0.2320	—	—	—	—
6s8p ^{1}P	—	—	—	—	—	—	—	—	—	—	—	—	—	−0.1427
5d6d ^{1}S	—	—	—	—	—	—	—	—	—	—	—	—	—	—
^{3}P	—	—	—	—	—	—	—	—	−0.0648	−0.0517	—	—	—	—
6s9p ^{1}P	—	—	—	—	—	—	—	—	—	—	—	—	—	−0.0749
6p7s ^{3}P	—	—	—	—	—	—	—	—	—	—	—	0.0562	0.0548	—
^{1}P	—	—	—	—	—	—	—	—	—	—	—	—	—	0.1393
6p6d ^{1}P	—	—	—	—	—	—	—	—	—	—	—	—	—	0.0919

Table 3. Configuration mixing coefficients used in the CCC calculations.

Level:	3	7	8	9	13	14	16	17	18	20	22	25	27	32
J:	2	2	2	1	2	2	3	2	1	2	2	1	2	1
6s5d ^{3}D	0.944	—	0.142	—	—	—	—	—	—	—	—	—	—	—
^{1}D	−0.133	—	0.886	—	—	—	—	0.084	—	—	—	—	—	—
6s6p ^{3}P	—	0.960	—	0.073	—	—	—	—	—	—	—	—	—	—
^{1}P	—	—	—	0.797	—	—	—	—	—	—	—	—	—	—
5d^2 ^{3}P	—	—	—	—	—	—	—	−0.287	0.799	0.745	—	—	—	—
^{1}D	0.033	—	—	—	—	—	—	0.740	—	0.286	—	—	—	—
^{3}F	—	—	—	—	—	—	—	−0.097	—	—	—	—	—	—
5d6p ^{3}P	—	−0.161	—	−0.012	—	—	—	—	—	—	−0.059	0.867	0.867	−0.091
^{1}P	—	—	—	−0.502	—	—	—	—	—	—	—	−0.056	—	−0.546
^{3}D	—	—	—	—	—	—	—	—	—	—	0.918	—	—	—
^{1}D	—	—	—	—	0.427	0.834	—	—	—	—	0.082	—	0.095	—
^{3}F	—	—	—	—	0.830	−0.427	0.933	—	—	—	—	—	—	—
^{1}F	—	—	—	—	—	—	−0.013	—	—	—	—	—	—	—
6s7p ^{3}P	—	—	—	—	—	—	—	—	—	—	—	−0.213	−0.213	0.683
^{1}P	—	—	—	—	—	—	—	—	—	—	—	0.071	—	0.023
6p^2 ^{3}P	—	—	—	—	—	—	—	—	0.389	0.363	—	—	—	—
^{1}D	—	—	—	—	—	—	—	0.324	—	0.125	—	—	—	—
5d6d ^{1}S	—	—	—	—	—	—	—	—	—	—	—	—	—	—
^{3}P	—	—	—	—	—	—	—	−0.165	0.458	0.427	—	—	—	—
^{1}D	—	—	—	—	—	—	—	−0.410	—	−0.158	—	—	—	—
6p7s ^{3}P	—	−0.116	—	−0.009	—	—	—	—	—	—	—	—	—	—
^{1}P	—	—	—	—	—	—	—	—	—	—	—	—	—	—
5d7s ^{3}D	−0.199	—	−0.030	—	—	—	—	—	—	—	—	—	—	—
^{1}D	0.033	—	−0.223	—	—	—	—	−0.111	—	—	—	—	—	—
5d7p ^{3}P	—	—	—	—	—	—	—	—	—	—	—	−0.391	−0.391	0.041
^{1}P	—	—	—	−0.255	—	—	—	—	—	—	—	0.034	—	0.329
^{3}D	—	—	—	—	—	—	—	—	—	—	−0.359	—	—	—
^{1}D	—	—	—	—	−0.131	−0.255	—	—	—	—	−0.025	—	−0.029	—
^{3}F	—	—	—	—	−0.256	0.132	−0.289	—	—	—	—	—	—	—
4f6s ^{3}F	—	—	—	—	0.115	−0.059	0.129	—	—	—	—	—	—	—

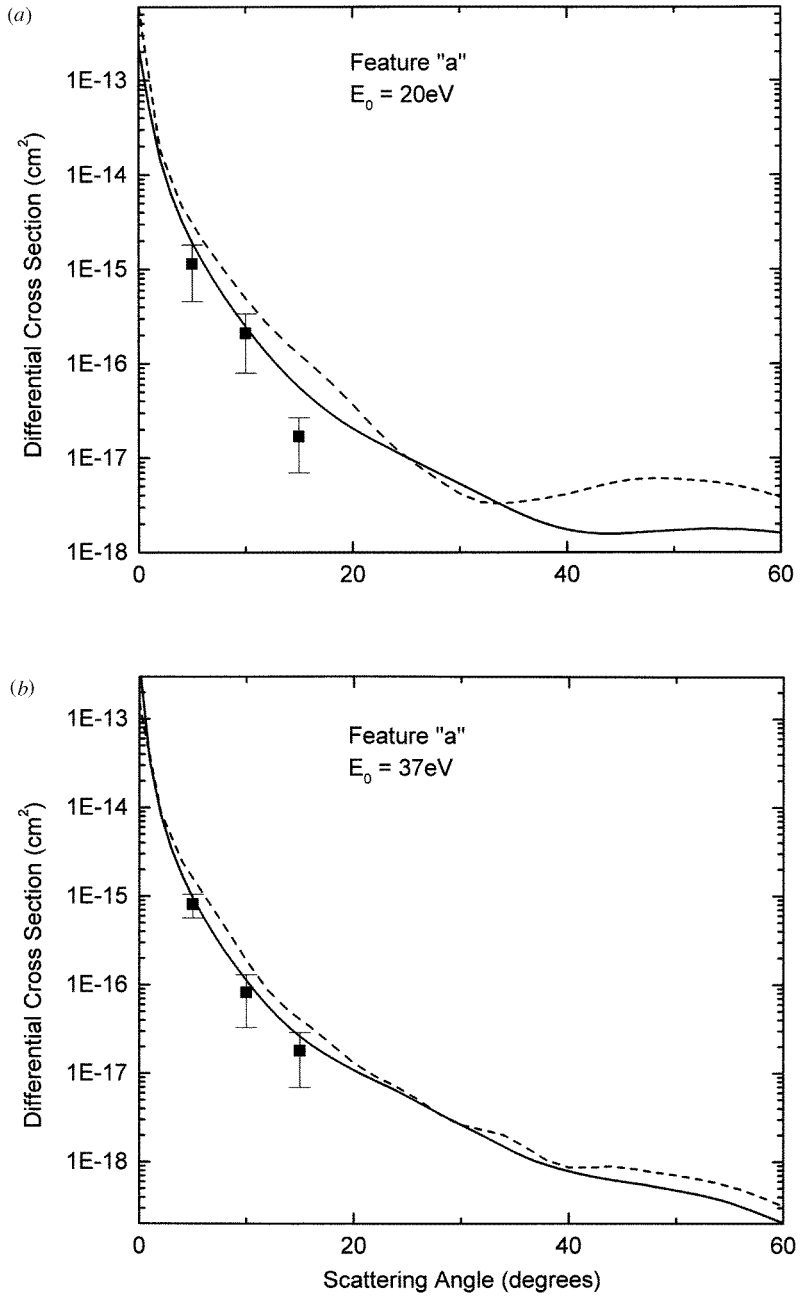

Figure 1. Measured and calculated DCS for feature 'a' (the 6s5d $^3D_2$–6s6p $^3P_2$ excitation). The full curve represents the CCC result. The broken curve represents the UDWA result. Measured data are represented by full squares with error bars. (*a*) Impact energy of 20 eV, (*b*) impact energy of 37 eV. (CCC calculations carried out at 35 eV.)

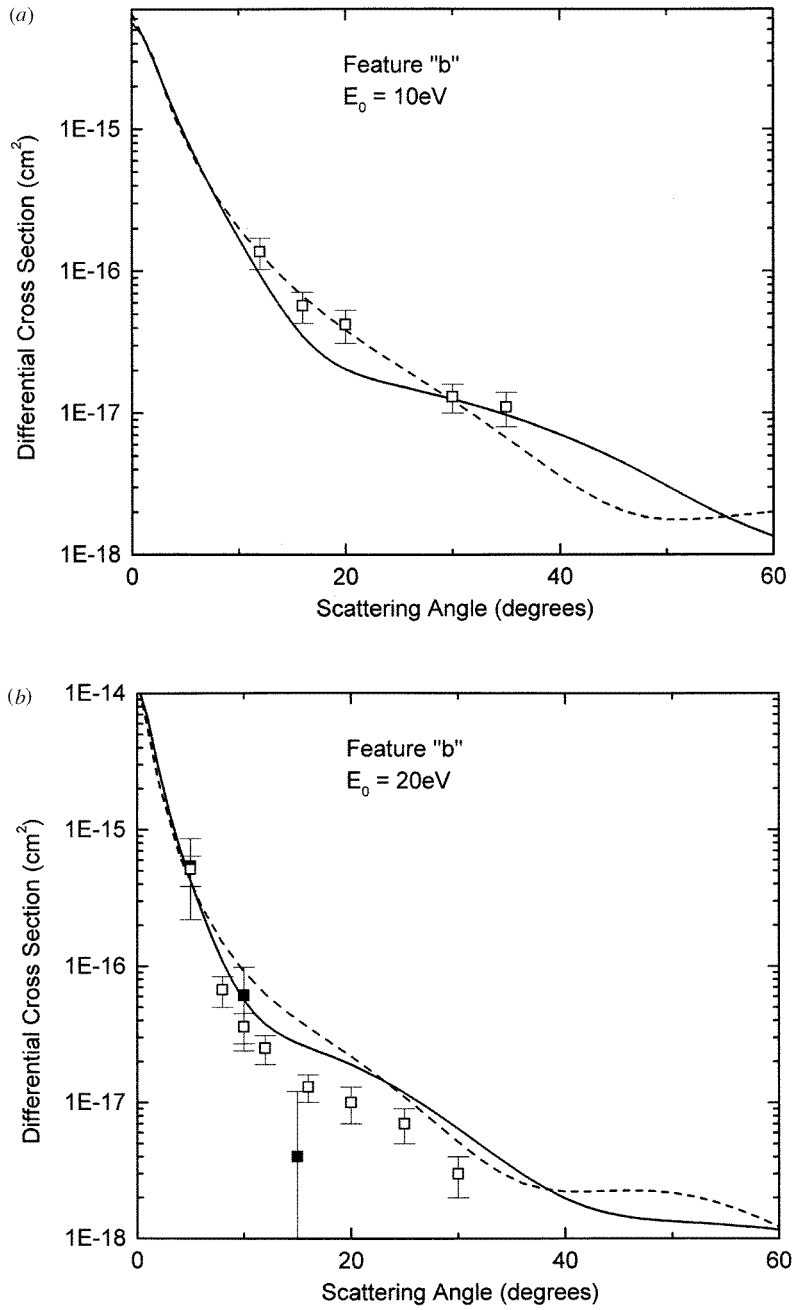

Figure 2. Measured and calculated DCS for feature 'b' (the 6s5d $^1D_2$–6s6p $^1P_1$ excitation). The full curve represents the CCC result. The broken curve represents the UDWA result. Measured data are represented by full squares with error bars. Measured data of Johnson *et al* (1999) are represented by open squares with error bars. (*a*) Impact energy of 10 eV, (*b*) impact energy of 20 eV and (*c*) impact energy of 37 eV. (CCC calculations carried out at 35 eV.)

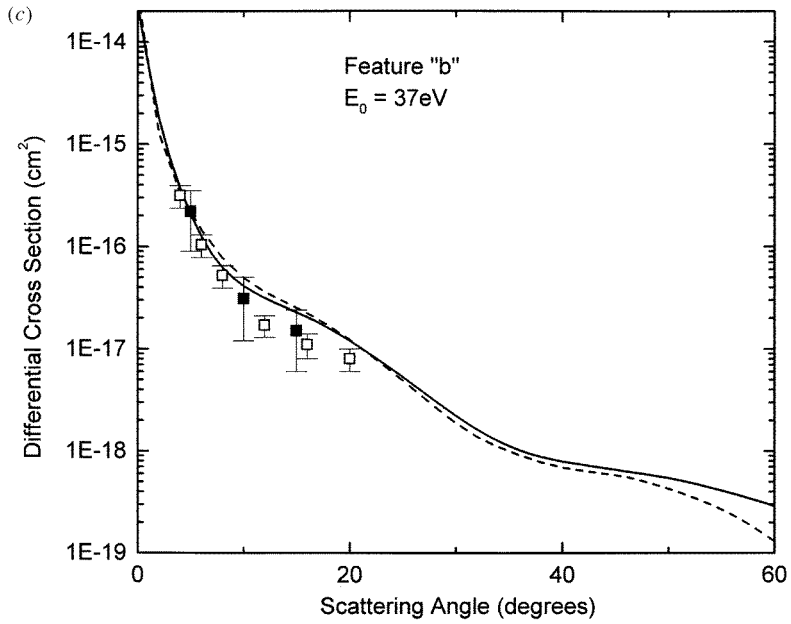

Figure 2. Continued.

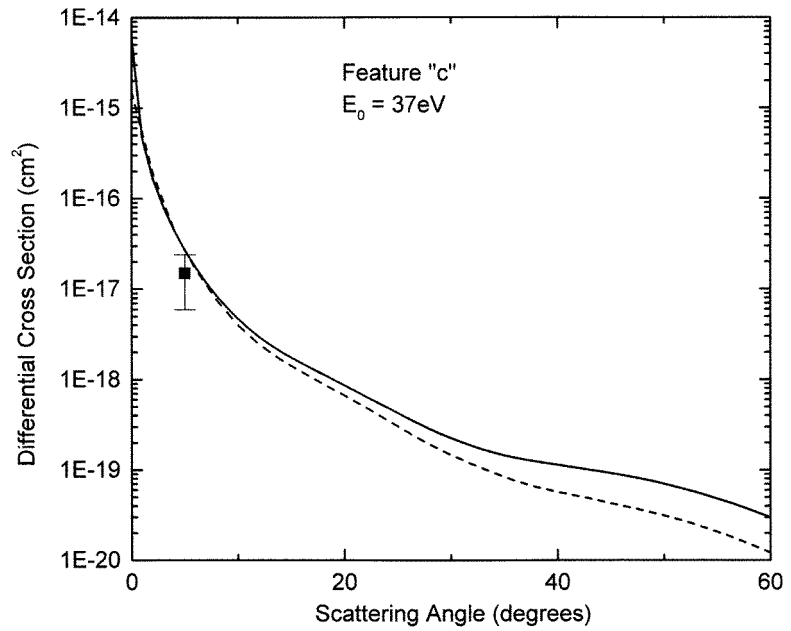

Figure 3. Measured and calculated DCS for feature 'c' (the 6s5d $^3D_2$–6s6p $^1P_1$ excitation). The full curve represents the CCC result. The broken curve represents the UDWA result. Measured data are represented by the full square with an error bar. Impact energy of 37 eV with the CCC calculations carried out at 35 eV.

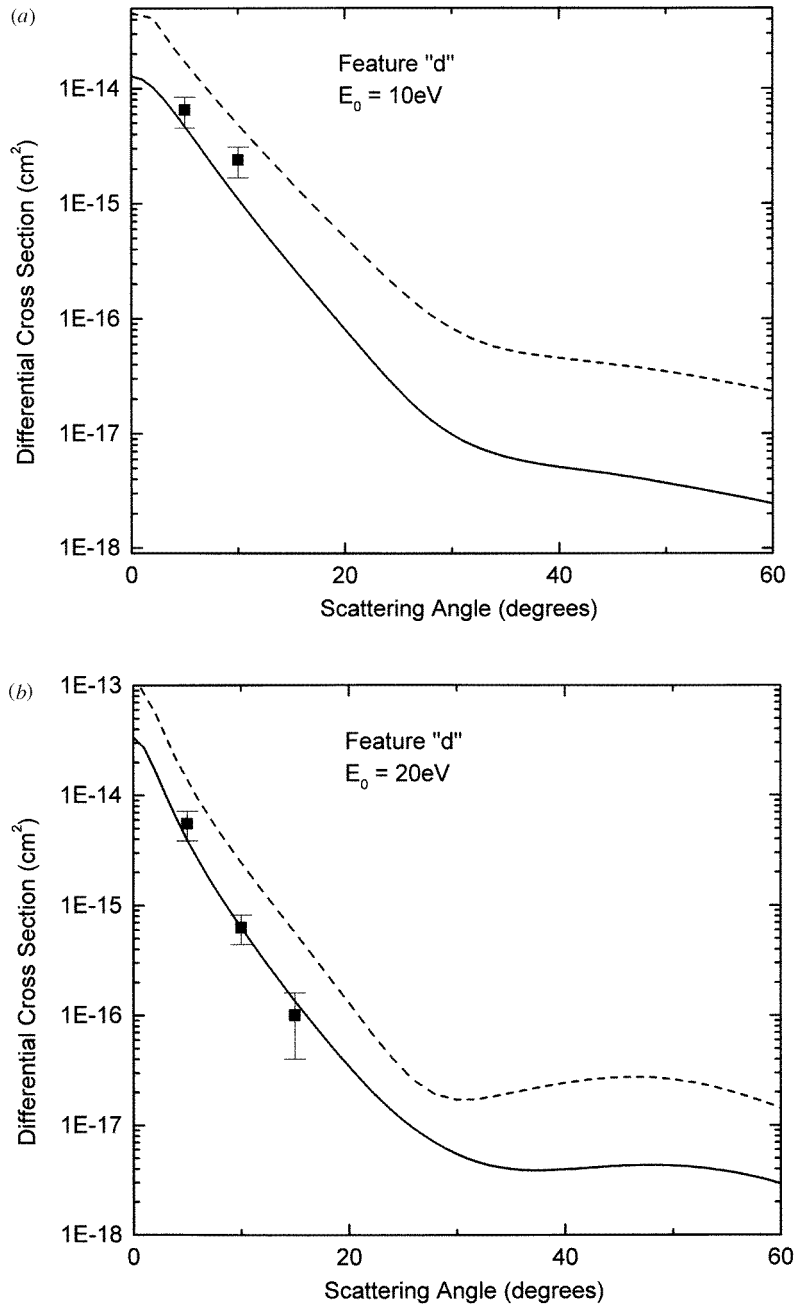

Figure 4. Measured and calculated DCS for feature 'd' (the 6s5d $^1D_2$–6s6p $^3F_2$ excitation). The full curve represents the CCC result. The broken curve represents the UDWA result. Measured data are represented by full squares with error bars. (*a*) Impact energy of 10 eV, (*b*) impact energy of 20 eV and (*c*) impact energy of 37 eV. (CCC calculations carried out at 35 eV.)

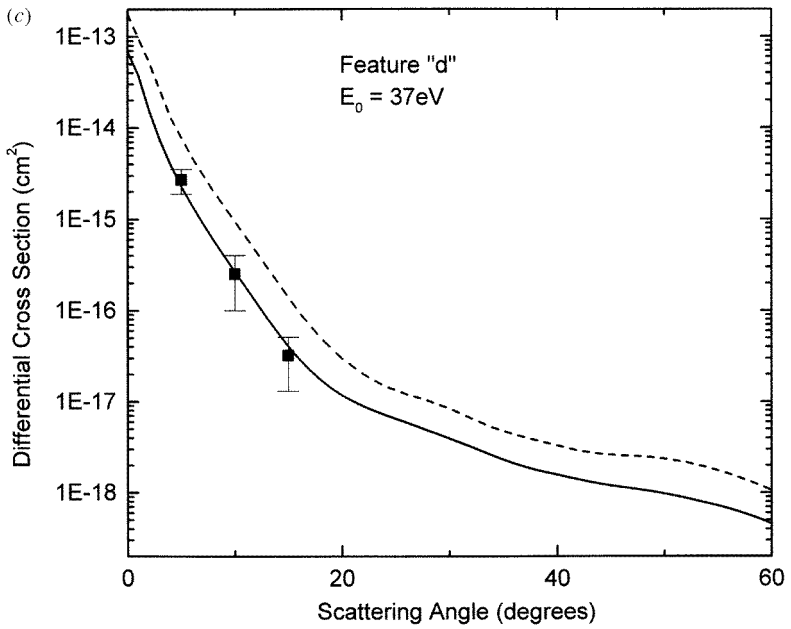

Figure 4. Continued.

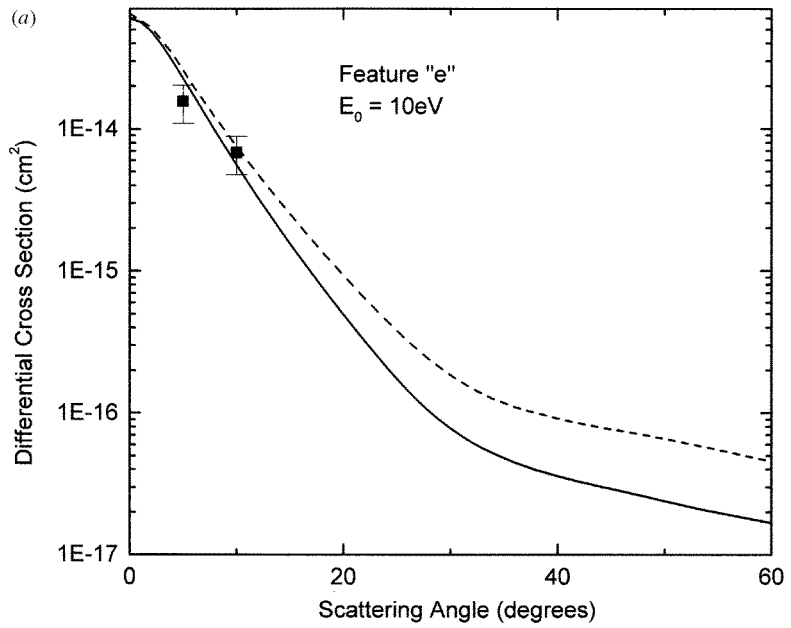

Figure 5. Measured and calculated DCS for feature 'e' (the combined 6s5d $^1D_2$–6p5d $^3F_3$, 6s5d $^1D_2$–5d^2 $^1D_2$, 6s5d $^1D_2$–6p5d $^1D_2$, 6s5d $^1D_2$–5d^2 $^3P_1$ excitations). The full curve represents the CCC result. The broken curve represents the UDWA result. Measured data are represented by full squares with error bars. (*a*) Impact energy of 10 eV, (*b*) impact energy of 20 eV and (*c*) impact energy of 37 eV. (CCC calculations carried out at 35 eV.)

Table 4. Differential cross sections.

	DCS (10^{-16} cm^2 sr^{-1})			
Feature	5°	10°	15°	20°
Impact energy: $E_0 = 10$ eV				
a	—	—	—	—
b	—	—	—	—
c	—	—	—	—
d	65.0(19.5)	24.0(7.2)	—	—
e	156.0(46.8)	68.0(20.4)	—	—
f	4.7(2.8)	2.6(1.6)	—	—
g	119.0(35.7)	28.0(8.4)	—	—
i_1	38.0(11.4)	13.0(3.9)	—	—
i_2	7.3(2.2)	3.7(2.2)	—	—
Impact energy: $E_0 = 20$ eV				
a	11.4(6.8)	2.1(1.3)	0.17(0.10)	—
b	5.4(3.2)	0.61(0.37)	0.04(0.08)	—
c	—	—	—	—
d	55.2(16.6)	6.3(1.9)	1.0(0.6)	—
e	158.6(47.6)	22.0(6.6)	3.9(2.3)	—
f	11.2(3.4)	1.8(1.1)	0.46(0.28)	0.29(0.17)
g	99.5(29.9)	20.0(6.0)	3.1(1.9)	—
i_1	52.2(15.7)	9.6(2.9)	1.2(0.7)	—
i_2	23.47(7.0)	3.3(2.0)	0.34(0.20)	—
Impact energy: $E_0 = 36.7$ eV				
a	8.1(2.4)	0.82(0.49)	0.18(0.11)	—
b	2.2(1.3)	0.31(0.19)	0.15(0.09)	—
c	0.15(0.09)	—	—	—
d	27(8.1)	2.5(1.5)	0.32(0.19)	—
e	84.0(25.2)	9.8(2.9)	1.7(1.0)	—
f	4.8(2.9)	0.60(0.36)	0.30(0.18)	—
g	71.3(21.4)	7.3(2.2)	1.3(0.8)	—
i_1	39.0(11.7)	3.8(2.3)	0.56(0.34)	—
i_2	18.0(5.4)	1.3(0.8)	0.09(0.06)	—

barium-atom energy levels and wavefunctions. The resulting configuration compositions are given in table 3. One-electron orbitals used in the CI expansion have been calculated by diagonalization of the Ba^+ ion Hamiltonian in a Sturmian (Laguerre) basis. The resulting barium target states are square integrable. Negative-energy states (relative to the Ba^+ ground state) represent an approximation to the barium discrete spectrum states, while positive-energy states provide square-integrable discretization of the barium continuum, therefore allowing coupling to the ionization channels.

To account for the polarizability of the inert core we have added phenomenological one- and two-electron polarization potentials. The cut-off parameters of the one-electron polarization potential have been chosen to fit the energies of the low-lying states of the Ba^+ ion. The set of two-electron configurations in the CI expansion has been constructed from one-electron orbitals with orbital angular momentum $l = 0, 1, 2$ and 3. One of the electrons in the configuration set has been restricted to occupy the Ba^+ 6s, 7s, 6p, 7p and 5d orbitals only, while the number of orbitals (within given l) for the other electron has been increased to achieve convergence in the description of the low-lying discrete states of the barium atom. We have found that such a choice of configurations is sufficient to account for a major part of

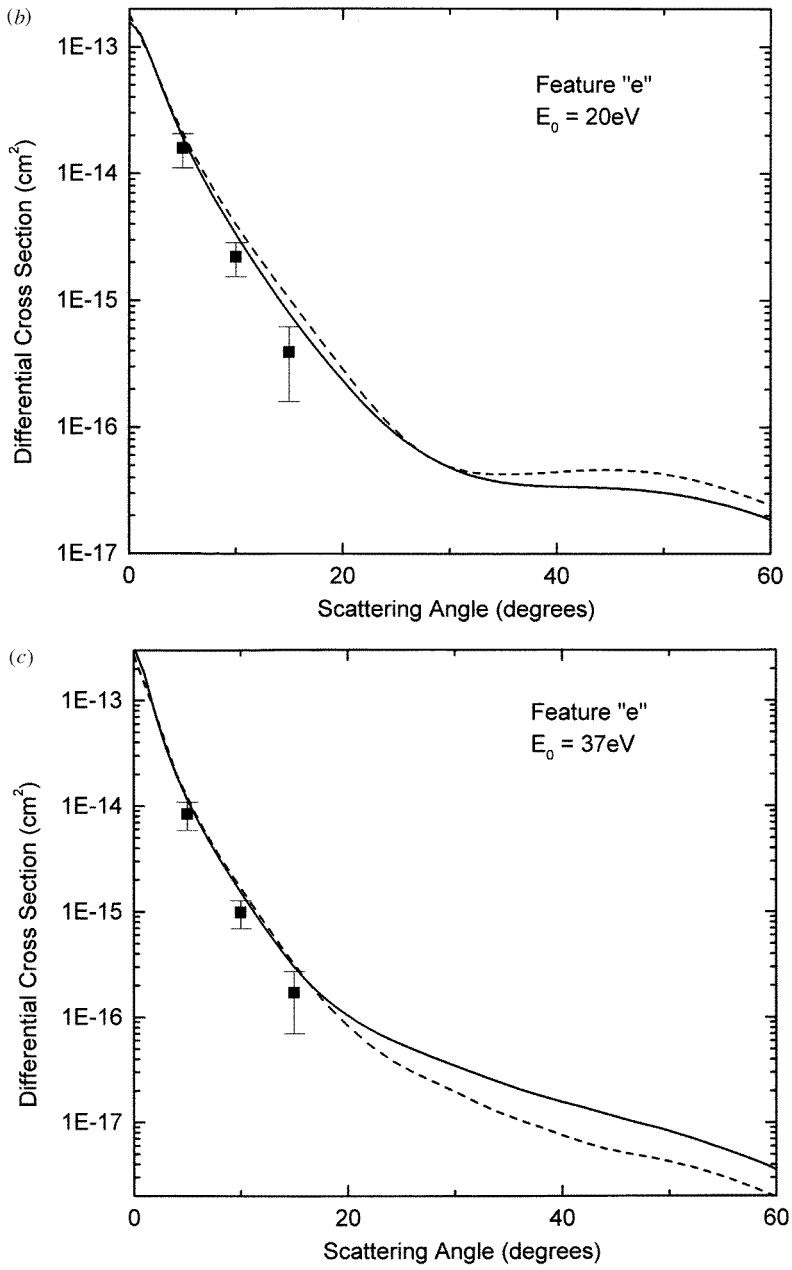

Figure 5. Continued.

the electron–electron correlations. The present calculation involved 115 states (14 ^{1}S, 17 ^{1}P^o, 19 ^{1}D^e, 19 ^{1}F^o, 7 ^{3}S, 9 ^{3}P^o, 9 ^{3}D^e, 9 ^{3}F^o and two each of ^{1,3}P^3, ^{1,3}D^o, ^{1,3}F^e) which included a large number of continuum, positive-energy states.

In order to compare the results of the non-relativistic CCC calculations with experiment we have used a technique essentially identical to the pair-coupling scheme that is used in the UDWA calculations. Namely, we first transform the non-relativistic CCC scattering amplitudes

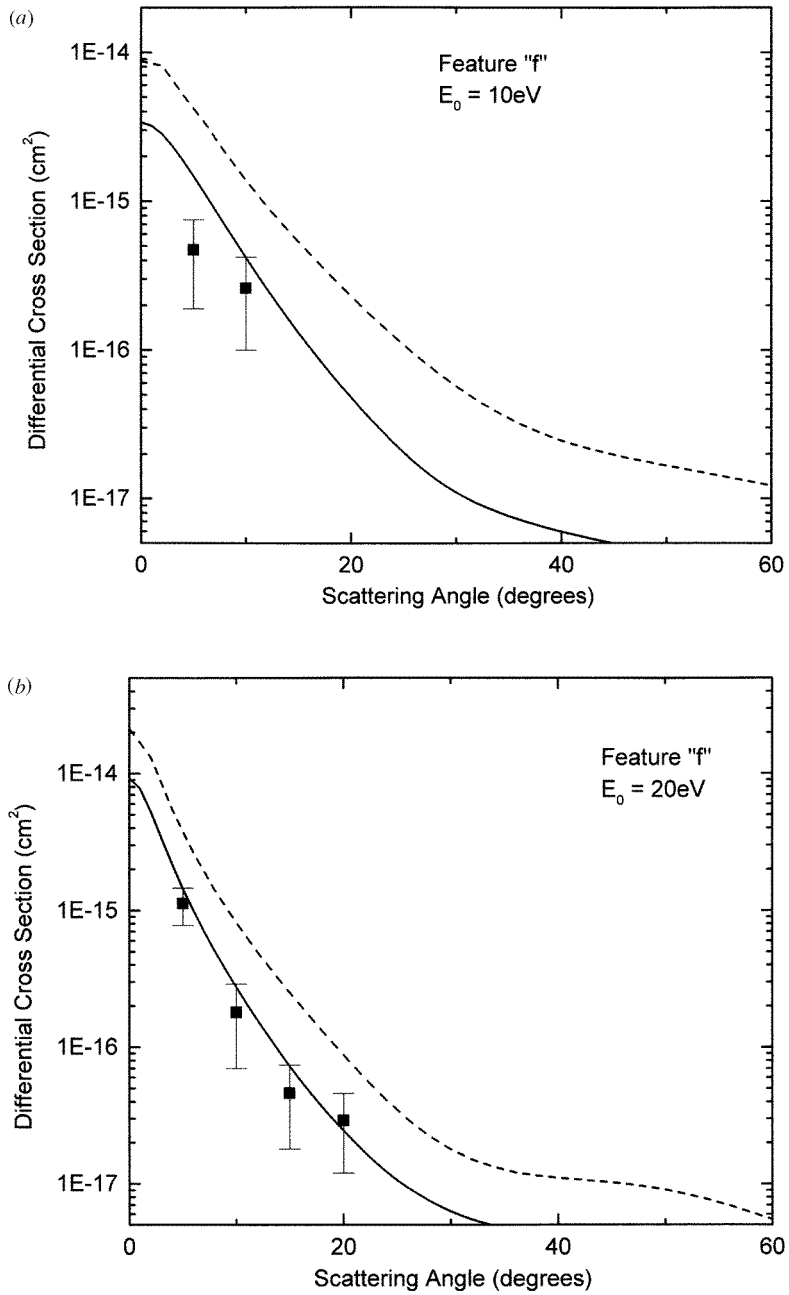

Figure 6. Measured and calculated DCS for feature 'f' (the combined $6s5d\ ^1D_2$–$5d^2\ ^3P_2$, $6s5d\ ^3D_2$–$6p5d\ ^3F_2$, $6s5d\ ^1D_2$–$6p5d\ ^1D_2$ excitations). The full curve represents the CCC result. The broken curve represents the UDWA result. Measured data are represented by full squares with error bars. (*a*) Impact energy of 10 eV, (*b*) impact energy of 20 eV and (*c*) impact energy of 37 eV. (CCC calculations carried out at 35 eV.)

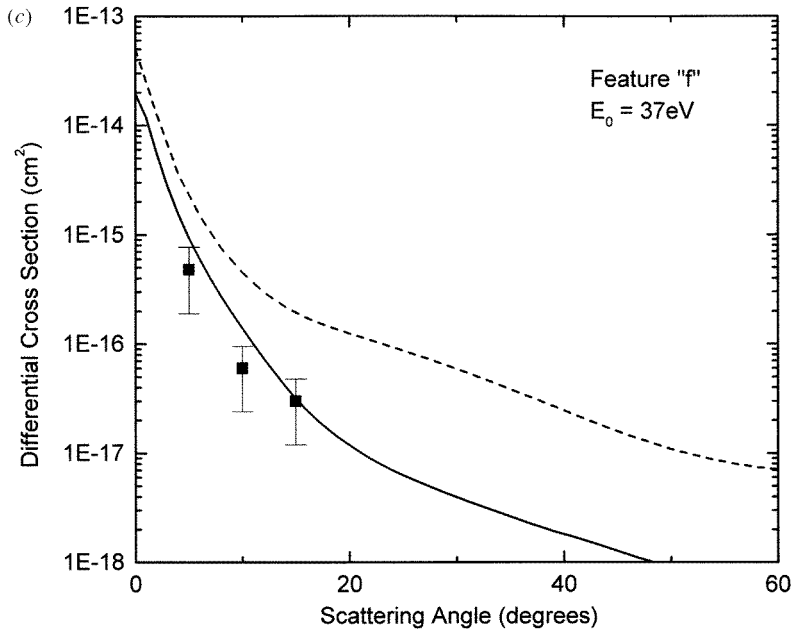

Figure 6. Continued.

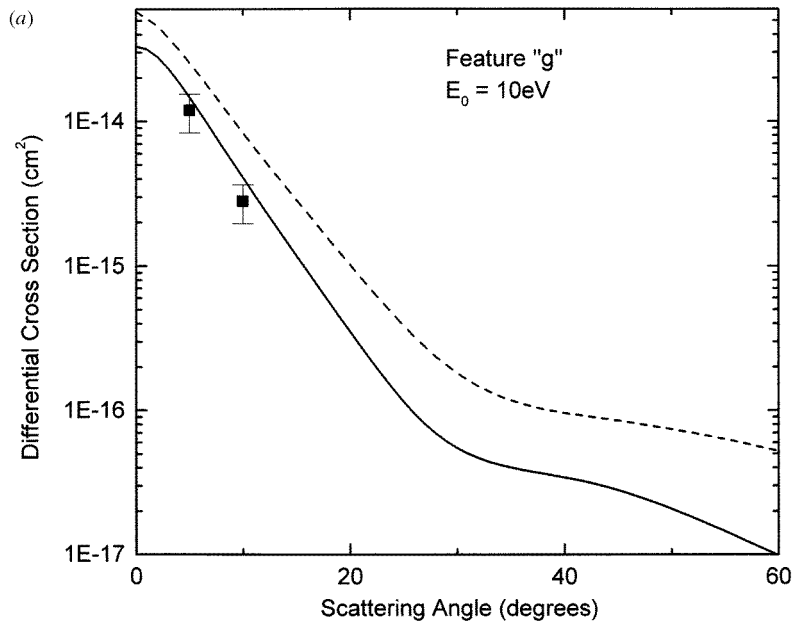

Figure 7. Measured and calculated DCS for feature 'g' (the combined 6s5d $^3D_2$–6p5d $^3F_3$, 6s5d $^3D_2$–5d^2 $^1D_2$, 6s5d $^3D_2$–6s5d $^1D_2$ excitations). The full curve represents the CCC result. The broken curve represents the UDWA result. Measured data are represented by full squares with error bars. (*a*) Impact energy of 10 eV, (*b*) impact energy of 20 eV and (*c*) impact energy of 37 eV. (CCC calculations carried out at 35 eV.)

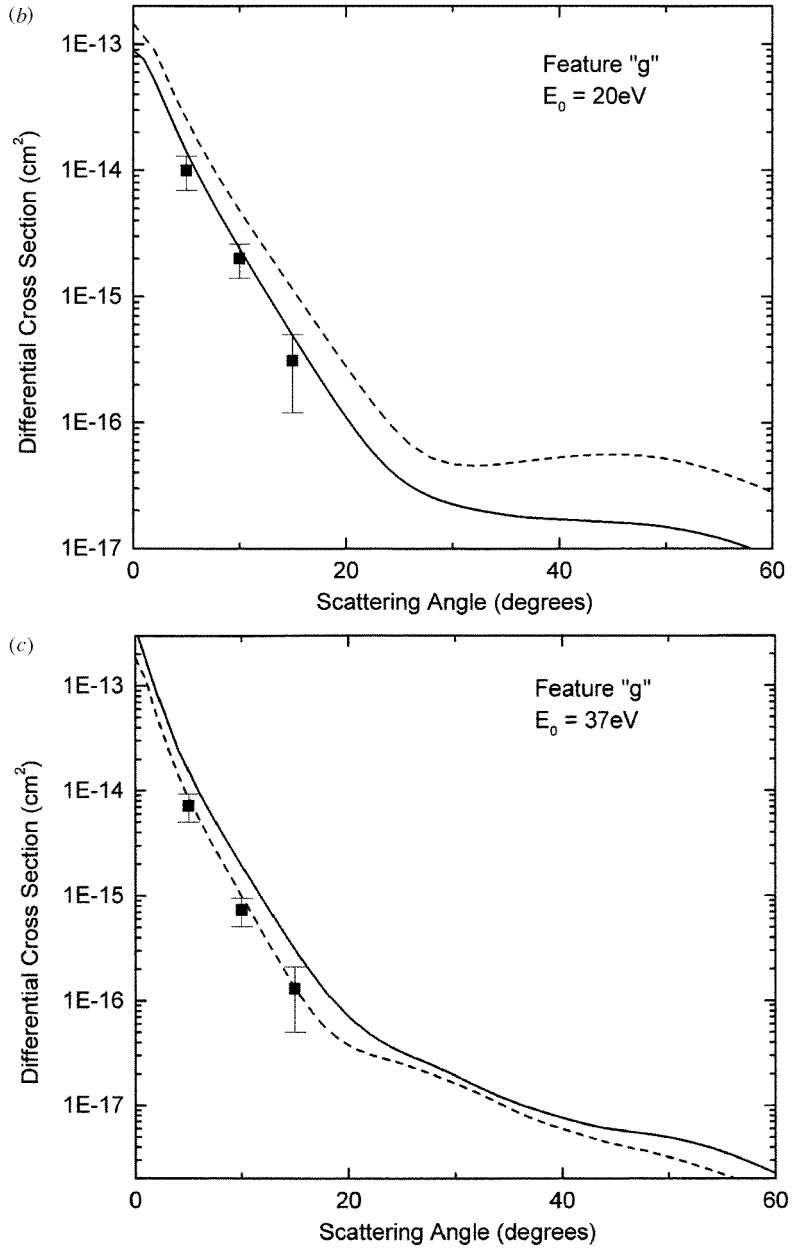

Figure 7. Continued.

$f^{S}_{\pi_f s_f l_f m_f, \pi_i s_i l_i m_i}$ (where the total spin is S, final (initial) target state parity is π_f (π_i), spin is s_f (s_i), orbital angular momentum is l_f (l_i), and its projection on the Z-axis of the collision frame is m_f (m_i)) to the amplitudes describing transitions between fine-structure levels J_f

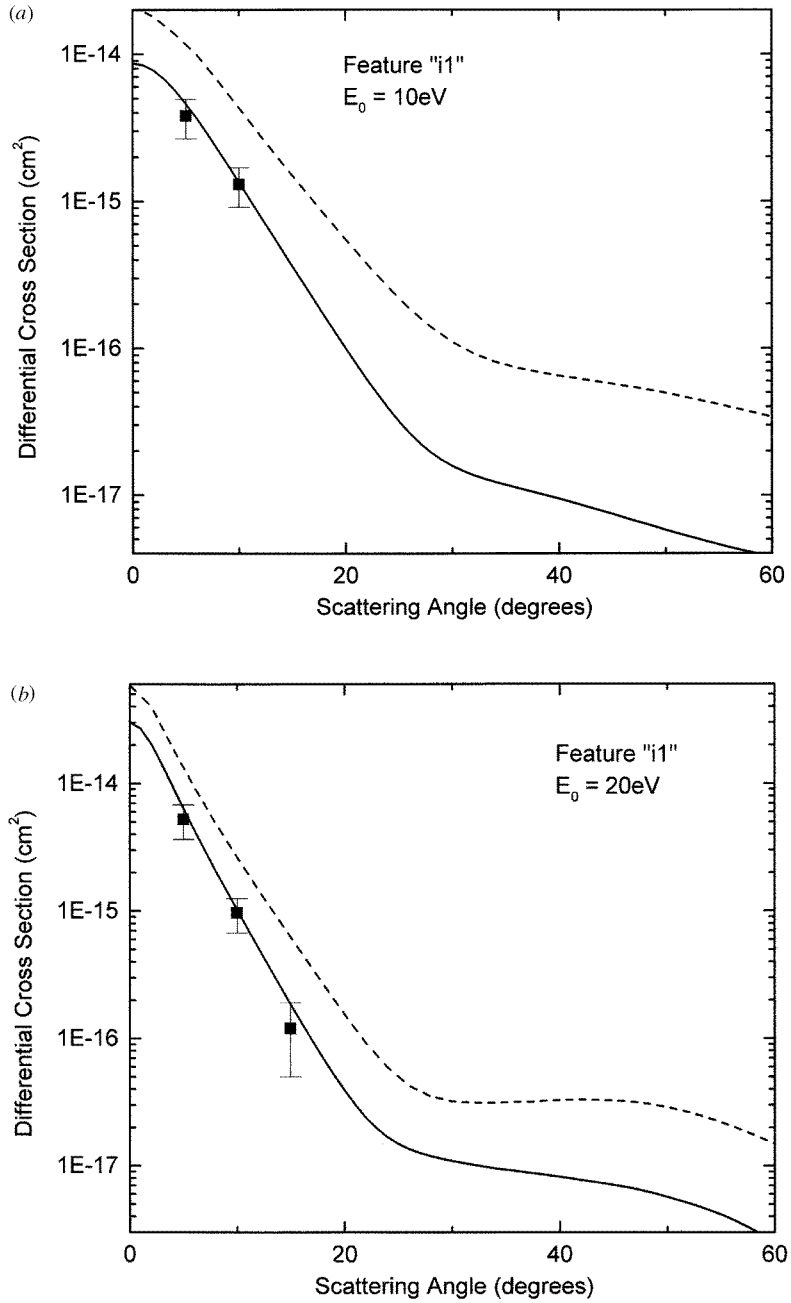

Figure 8. Measured and calculated DCS for feature 'i_1' (the combined 6s5d $^3D_2$–6p5d $^3P_1$, 6s5d $^3D_2$–6p5d $^3P_2$ excitations). The full curve represents the CCC result. The broken curve represents the UDWA result. Measured data are represented by full squares with error bars. (*a*) Impact energy of 10 eV, (*b*) impact energy of 20 eV and (*c*) impact energy of 37 eV. (CCC calculations carried out at 35 eV.)

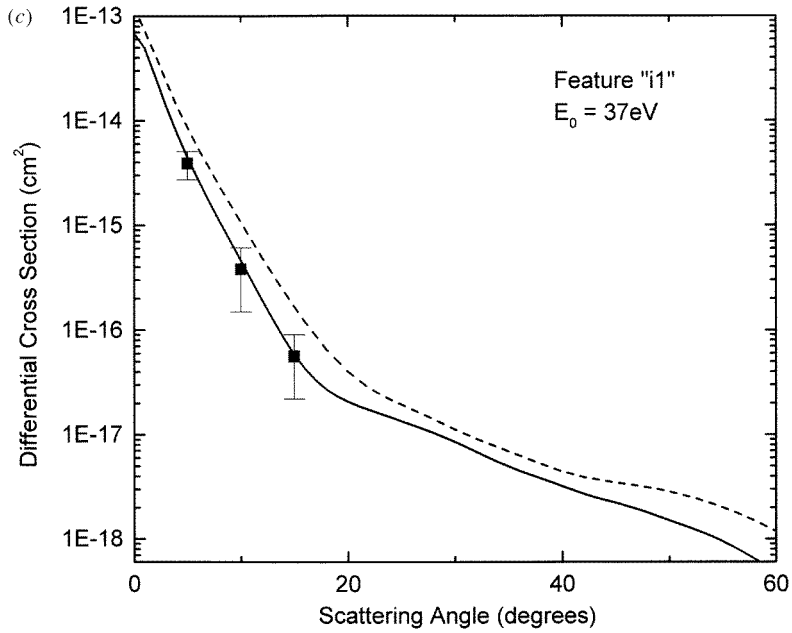

Figure 8. Continued.

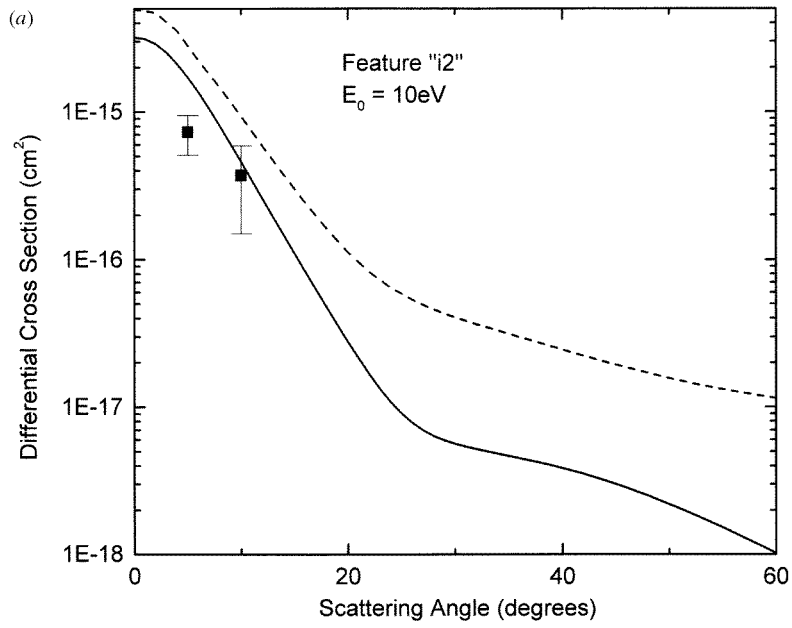

Figure 9. Measured and calculated DCS for feature 'i_2' (the 6s5d $^1D_2$–6s7p $^1P_1$ excitation). The full curve represents the CCC result. The broken curve represents the UDWA result. Measured data are represented by full squares with error bars. (*a*) Impact energy of 10 eV, (*b*) impact energy of 20 eV and (*c*) impact energy of 37 eV. (CCC calculations carried out at 35 eV.)

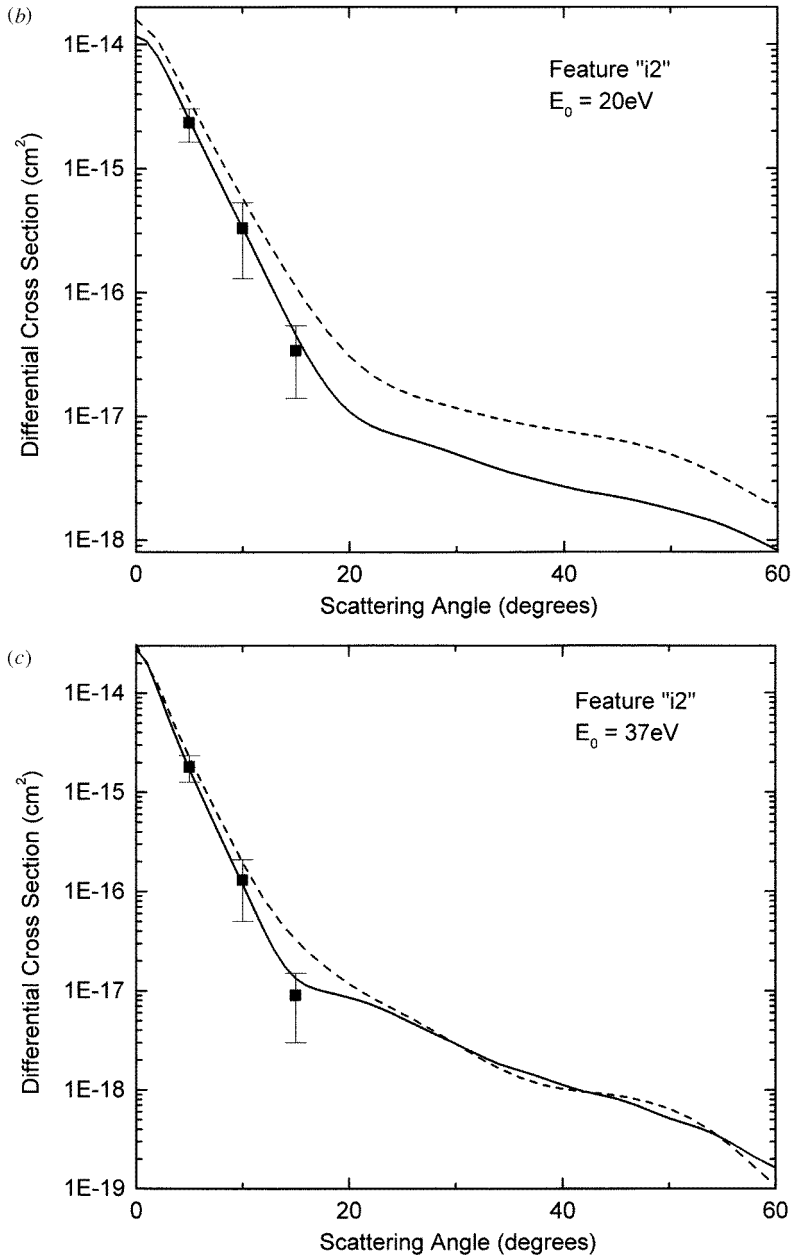

Figure 9. Continued.

and J_i, respectively,

$$f^{\sigma_f,\sigma_i}_{\pi_f J_f M_f,\pi_i J_i M_i}(\gamma_f,\gamma_i) = \sum_{m_f,q_f,m_f,q_f,S} C^{J_f M_f}_{l_f m_f,s_f q_f} C^{SM_S}_{\frac{1}{2}\sigma_f,s_f q_f} C^{J_i M_i}_{l_i m_i,s_i q_i} C^{SM_S}_{\frac{1}{2}\sigma_i,s_i q_i} f^{S}_{\pi_f s_f l_f m_f,\pi_i s_i l_i m_i}. \tag{9}$$

Here σ_f and σ_i are final (initial) projectile spin projections on the Z-axis of the collision frame

and the index γ distinguishes states with the same orbital angular momentum, spin and parity. The above amplitudes are used to form amplitudes in the intermediate coupling scheme

$$F^{\sigma_f,\sigma_i}_{\pi_f J_f M_f,\pi_i J_i M_i}(\beta_f,\beta_i) = \sum_{\gamma_f,\gamma_i} C^{\beta_f}_{\gamma_f} C^{\beta_i}_{\gamma_i} f^{\sigma_f,\sigma_i}_{\pi_f J_f M_f,\pi_i J_i M_i}(\gamma_f,\gamma_i) \tag{10}$$

where the index β distinguishes target states with the same total angular momentum J and parity π. We obtain mixing coefficients C^{β}_{γ} by diagonalizing the Breit–Pauli Hamiltonian (only the one-body spin–orbit term is used) in the basis of the barium target states obtained from the non-relativistic barium structure calculation described above.

4. Results and discussion

Measured DCS are presented in table 4 and compared with the UDWA and CCC theories in figures 1–9. Error limits on the measured values reflect contributions of

(a) 10% for strong features and 50% for weak features, in the determination of relative scattering intensities by means of our spectrum unfolding procedure;
(b) 25% in the $^1S_0$–$^1P_1$ DCS used for normalization;
(c) 10% in the determination of excited-state populations; and
(d) 10% in the assumption of an isotropic (unaligned) atomic target.

With these uncertainties, added in quadrature, we are left with a possible 60% error for weak features and a possible 30% error for strong features.

Figures 1–9 show that, in all cases, the calculations reveal a forward-peaking behaviour of the DCS, characteristic of dipole-allowed excitations. The presence of a dipole-allowed contribution to all the excitations studied is not surprising because of the breakdown of LS coupling in target levels 3 (nominally $^3D_2$) and 8 (nominally $^1D_2$). From tables 2 and 3 it is apparent that these levels have a mixed singlet–triplet character and are best described by intermediate coupling.

In a comparison of the experimental data with CCC theory we find excellent agreement in all cases. Results of the UDWA calculations at 37 eV impact energy are in relatively close agreement with CCC results and experimental data except for the d and f features which are significantly dipole-forbidden in nature. In general, the effectiveness of the UDWA approach worsens somewhat with decreasing impact energy but good agreement is still obtained for the strongly dipole-allowed excitations (features a, b, e and i2) at the lower impact energies. There is a general tendency for the UDWA calculations to overestimate the DCS at lower energies.

Based upon the present observations, we conclude that the CCC calculations can be reliably used for generating cross sections for excitations out of the Ba metastable levels. Since experimental determination of these cross sections for a large number of scattering channels and over wide ranges of impact energy and scattering angle will not be readily available, reliance on theoretical results is necessary and the CCC approach has been demonstrated to be suitable for this purpose.

Acknowledgments

The measurements were carried out at the Jet Propulsion Laboratory and were supported by the US National Science Foundation and by the US National Aeronautics and Space Administration. Work at the Los Alamos Laboratory has been performed under the auspices of the US Department of Energy. DF and IB acknowledge the support of the Australian Research Council and the Flinders University of South Australia. They also wish to express

their indebtedness to the South Australian Centre for High Performance Computing and Communications. PWZ acknowledges financial support from the Natural Sciences and Engineering Research Council of Canada.

References

Allen L H 1984a *Physics of Thermal Gaseous Nebulae* (*Astrophysics and Space Science Library* vol 112 (Boston, MA: Reidel) pp 26–30, 116–46
Azizi M, Wülker C, Hink W and Sandner W 1994 *Z. Phys.* D **30** 161
Bizzarri A and Huber M C E 1990 *Phys. Rev.* A **42** 5422
Blum K 1981 *Density Matrix Theory and Applications* (New York: Plenum)
Brinkmann R T and Trajmar S 1981 *J. Phys. E: Sci. Instrum.* **14** 245
Clark R E H 1978 *Comput. Phys. Commun.* **16** 119
Cowan R D 1968a *J. Opt. Soc. Am.* **58** 808
——1968b *J. Opt. Soc. Am.* **58** 925
——1981 *Theory of Atomic Spectra* (Berkeley, CA: University of California Press)
Cowan R D and Griffin D C 1967 *J. Opt. Soc. Am.* **66** 1010
Davis J, Kepple P C and Bleha M 1976 *J. Quant. Spectrosc. Radiat. Transfer* **16** 1043
Delcroix P, Ferreira C M and Ricard A 1976 Metastable atoms and molecules in ionized gases *Principles of Laser Plasmas* ed G Bekefi (New York: Wiley) ch 5
Fursa D V and Bray I 1997 *J. Phys. B: At. Mol. Opt. Phys.* **30** 5895
——1999 *Phys. Rev.* A **59** 282
Jensen S, Register D and Trajmar S 1978 *J. Phys. B: At. Mol. Phys.* **11** 2367
Johnson P V, Eves B, Zetner P W, Fursa D and Bray I 1999 *Phys. Rev.* A **59** 439
Johnston M, Fujii K, Nickel J and Trajmar S 1996 *J. Phys. B: At. Mol. Opt. Phys.* **29** 531
Kelly F M and Mathur M S 1977 *Can. J. Phys.* **55** 83
Korenman G Ya 1975 *Sov. J. Nucl. Phys.* **21** 398
Krivchenkova V S and Khakaev A D 1975 *Opt. Spectrosc.* **39** 123
Li Y and Zetner P W 1995 *J. Phys. B: At. Mol. Opt. Phys.* **28** 5151
——1996 *J. Phys. B: At. Mol. Opt. Phys.* **29** 1803
Lin Chun C and Anderson L W 1992 *Adv. At. Mol. Opt. Phys.* **29** 1
Macek J and Hertel I V 1974 *J. Phys. B: At. Mol. Phys.* **7** 2173
Mann J B 1983 *At. Data Nucl. Data Tables* **29** 407
Massey H S W, McDaniel E W and Bederson B (eds) 1982a *Special Topics* (*Applied Atomic Collision Physics* vol 5) (New York: Academic)
——1982b *Atmospheric Physics and Chemistry* (*Applied Atomic Collision Physics* vol 1) (New York: Academic)
——1982c *Gas Lasers* (*Applied Atomic Collision Physics* vol 3) (New York: Academic)
Miles B M and Wiese W L 1969 *Atomic Data* vol 1 (reprinted 1980 *National Standard Reference Data Series* (*US National Bureau of Standards (US) Circular no 68*) (Washington, DC: US Govt Printing Office))
Moore C 1958 *Atomic Energy Levels as Derived from Analysis of Optical Spectra* (*US National Bureau of Standards Circular 467*) vol III (Washington, DC: Govt Printing Office)
Register D F, Trajmar S, Csanak G, Jensen S W, Fineman M A and Poe R T 1983 *Phys. Rev.* A **28** 151
Saraph H 1972 *Comput. Phys. Commun.* **3** 256
Saraph H, Seaton M J and Shemming J 1969 *Phil. Trans. R. Soc.* **264** 77
Shafranyosh I I, Snegurskaya T A, Margitich N A, Bogacheva S P, Lengyel V I and Zatsarinny O I 1997 *J. Phys. B: At. Mol. Opt. Phys.* **31** 2261
Trajmar S, Kanik I, Khakoo M A, LeClair L R, Bray I, Fursa D and Csanak G 1998 *J. Phys. B: At. Mol. Opt. Phys.* **31** L393
——1999 *J. Phys. B: At. Mol. Opt. Phys.* **32** at press
Trajmar S and Nickel J C 1992 *Adv. At. Mol. Opt. Phys.* **30** 45
Wang S, Trajmar S and Zetner P 1994 *J. Phys. B: At. Mol. Opt. Phys.* **27** 1613
Zetner P W, Trajmar S and Csanak G 1990 *Phys. Rev.* A **41** 5980
Zetner P W, Trajmar S, Wang S, Kanik I, Csanak G, Clark R E H, Abadallah J Jr and Nickel J C 1997 *J. Phys. B: At. Mol. Opt. Phys.* **30** 5317